Journal of the European Ceramic Society **16** (1996) 1041–1050

PII: S0955-2219(96)00037-4
0955-2219/96/$15.00

Fabrication and Crystal Chemistry of $Bi_{3/2}ZnSb_{3/2}O_7$ Pyrochlore

A. Mergen & W. E. Lee*

University of Sheffield, Department of Engineering Materials, Sheffield S1 3JD, UK

(Received 20 July 1995; revised version received 18 January 1996; accepted 23 January 1996)

Abstract

$Bi_{3/2}ZnSb_{3/2}O_7$ pyrochlore was prepared both by conventional solid-state reaction of mixed oxides and by a coprecipitation method, and the reaction sequence to pyrochlore via both methods was investigated. In the mixed oxide powder pyrochlore is formed above 700°C with the appearance of $24Bi_2O_3.ZnO$ ($Bi_{48}ZnO_{73}$) compound at about 550°C due to the heterogeneity of the powder compact. Coprecipitated powder reacts directly to give pyrochlore at around 550°C without formation of any additional compound due to the atomic-scale mixing In the $Bi_{3/2-x/2}Zn_{1+x}Sb_{3/2-x/2}O_{7-x}$ pyrochlore system with zinc concentration between x = 0·1 and x = 1·2, Zn incorporation to replace Bi and Sb led to formation of spinel and Bi-rich liquid along with pyrochlore of undefined composition.

1 Introduction

The crystal structure of the mineral pyrochlore, $(Ca,Na)_2(Nb,Ta)_2(OH,F)_7$, was first determined by von Gaertner[1] to belong to the space group *Fd3m* (No. 227 in Volume 1 of the International Tables of X-ray Crystallography). Since then a large number of compounds have been discovered with this type of crystal structure, including many with potentially useful electrical properties. Interest in electrical pyrochlores has been high since Cook and Jaffe[2] discovered that $Cd_2Nb_2O_7$ was ferroelectric with a peak dielectric constant of about 1200.

The crystal structure of pyrochlore may be regarded as an anion-deficient fluorite structure in which the cations form a face-centred cubic array and the anions assume an ordered arrangement in the tetrahedral interstices of the cation array.[2] As well as being a fluorite derivative, the crystal structure of pyrochlore has been described as two interpenetrating cristobalite-like networks[3] and as a network of BX_6 octahedra (where B is a sixfold coordinated cation and X is an anion) linked corner to corner with the A cations filling the interstices.[4] These different descriptions arise because the cation coordination polyhedra change shape with the value of the anion positional parameter, x. The general formula for pyrochlore compounds is $A_2B_2X_7$ (whereas fluorite would be $A_2B_2X_8$) with large A-type cations in eightfold coordination, smaller B-type cations in sixfold coordination and X-type anions. Two different anion positions occur so that the general formula can be written $A_2B_2X_6Z$, with the X anions having two A and two B near neighbours and the Z anion having only A near neighbours. As the mineral formula indicates, multiple cation/anion replacements are possible.

Pyrochlores can be classified according to the ion sites and valency as *normal* $A_2^{3+}B_2^{4+}X_7$, $A_2^{2+}B_2^{5+}X_7$, types or, by removing combinations of A and Z ions, a variety of *defect* pyrochlores occur with non-stoichiometry on cation or anion sites. Defect pyrochlores have the general formula $A_{2-x}B_2X_6Z_y$ ($0 \leq x \leq 1$ and $0 \leq y \leq 1$) giving, for example, AB_2X_6, $A_2B_2X_6Z_{1-y}$. However, an enormous range of ions of various valencies can be substituted into the pyrochlore structure so that it is difficult to fully classify them. For example, the pyrochlore of interest in the present work is believed to be $Bi_{1.5}^{3+}Zn^{2+}Sb_{1.5}^{5+}O_7$.[5]

Normal $A_2^{3+}B_2^{4+}X_7$-type pyrochlores are the most common due to the many suitable A and B cations. An excellent review of the pyrochlore structure is given by Subramanian *et al.*[6]

Pyrochlore compounds have many potential applications due to their electrical, dielectric, magnetic, optical and catalytic properties. For example, $R_2Zr_2O_7$ (R = rare earth) pyrochlores have possible applications as fluorescence centre hosts, high-temperature heating elements and oxidation catalysts. $Bi_2Ru_2O_7$ pyrochlore, suitably modified by solid solution with $Cd_2Nb_2O_7$, has been suggested as a thermistor material and $Gd_2(Zr_xTi_{1-x})O_7$ is a prospective solid oxide fuel cell electrolyte. While these applications are for ceramics where the pyrochlore is the major phase, they may also occur in the microstructure as a second

* To whom correspondence should be addressed.

phase, where frequently they degrade the desired electrical behaviour. For example, many $Pb(A_xB_{1-x})O_3$ perovskite relaxor ferroelectrics such as $PbMg_{1/3}Nb_{2/3}O_3$ (PMN) contain pyrochlore as an unwanted intermediate polymorph. The transformation to the desired perovskite crystal structure is slow and the two polymorphs coexist with the non-ferroelectric pyrochlore dramatically reducing the dielectric constant.

ZnO varistors are composed of ZnO grains, Bi_2O_3-containing grain boundaries responsible for the non-linear response, and intergranular phases such as $Bi_{3/2}ZnSb_{3/2}O_7$ (BZS) pyrochlore and $Zn_7Sb_2O_{12}$ spinel.[7] In the pure $ZnO–Bi_2O_3–Sb_2O_3$ system pyrochlore forms above 650°C and melts at 1280°C. Inada[8] found that pyrochlore forms and disappears on heating [reaction(1)] but may be reproduced on slow cooling [reaction (2)]:

$$4Bi_{3/2}ZnSb_{3/2}O_7 + 17ZnO \xrightarrow{950–1050°C} 3Zn_7Sb_2O_{12} + 3Bi_2O_3 \quad (1)$$

$$3Zn_7Sb_2O_{12} + 3Bi_2O_3 \xrightarrow{950–850°C} 4Bi_{3/2}ZnSb_{3/2}O_7 + 17ZnO \quad (2)$$

The pyrochlore is undesirable in ZnO varistor systems since it ties up some of the Bi_2O_3 that would otherwise migrate to grain boundaries and provide the non-linear response and also because the ZnO–pyrochlore interphase boundaries do not show a non-linear response.[9]

If the α-spinel polymorph is stabilized by adding e.g. Co, Mn and Cr, which dissolve in the bismuth oxide liquid and appear in the spinel crystal structure,[7] reaction (2) will not occur. The amount of pyrochlore formed on slow cooling, therefore, depends on the additives present and can be reduced to low levels in commercial systems.

$Bi_{3/2}ZnSb_{3/2}O_7$ has been fabricated from solid-state reaction of mixed oxide powders and via powder produced by a coprecipitation method. Thermal analysis and X-ray diffraction have been used to investigate the reaction sequence and the microstructural evolution has been determined using electron microscopy. Moreover, the effect of Zn replacing Bi and Sb in the $Bi_{3/2}ZnSb_{3/2}O_7$ pyrochlore phase has been examined.

2 Experimental

$Bi_{3/2}ZnSb_{3/2}O_7$ pyrochlore powder was prepared both by solid-state reaction of bismuth oxide (Bi_2O_3, >99·9%), zinc oxide (ZnO, >99·9%) and antimony oxide (Sb_2O_3, >99%) powders,* which were wet-mixed and milled in ethanol for 4 h using zirconia balls before drying, and by a coprecipitation route involving preparation of cation solutions from antimony chloride ($SbCl_3$, >99·5%), zinc chloride ($ZnCl_2$, >98%) and bismuth oxide (Bi_2O_3, >99·9%). Figure 1 shows block diagrams of the main steps in the processing routes via mixed oxide [Fig. 1(a)] and coprecipitation [Fig. 1(b)]. In the coprecipitation route the starting materials were dissolved in HCl/H_2O by using excess acid and poured into KOH solution to give a pH of >12, which is neces-

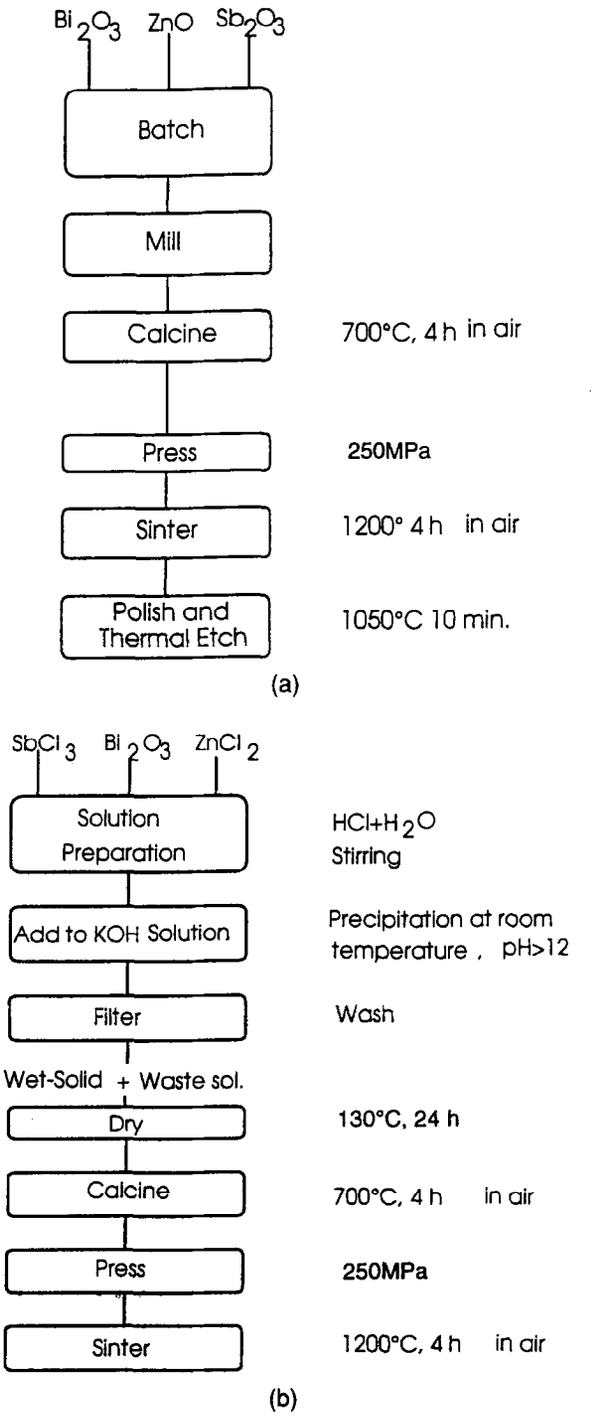

Fig. 1. The processing route for (a) mixed oxide powder and (b) coprecipitated powder.

* All chemicals were supplied by Aldrich Chemical Company Ltd, Dorset, UK.

sary to precipitate the pyrochlore powder. Bismuth and antimony metal salts could be precipitated at low pH values of between 1 and 2 with KOH.[7,10,11] Both of these hydroxides are weak bases and the salts of these metals are hydrolysed by water, yielding insoluble salts such as BiOCl and SbOCl.[12] Consequently, on preparing pyrochlore solution, excess acid is used to stabilize the solution of Bi and Sb.[12,13] However, zinc chloride could be precipitated with KOH at high pH values of around 10, giving zinc hydroxide.[7,11] Precipitates were removed from the solution by centrifuge and washed several times with distilled water. Wet-mixed oxide and coprecipitated powders were dried at 130°C for 24 h. Both dried mixed oxide and coprecipitated powders were calcined for 4 h at 700°C. After calcination the coprecipitated powder was ball-milled for 4 h in ethanol to break up the agglomerates. Chemical analysis of the natant solution remaining after precipitation was performed by inductively coupled plasma atomic emission spectrometry (ICP-AES).

The phase development in dried but uncalcined powders was examined using differential thermal analysis (DTA) and thermogravimetric analysis (TGA) at a heating rate of 10 K min^{-1} in air. In addition, pellets 10 mm diameter × ~1 mm thick were uniaxially pressed at 250 MPa from uncalcined powder, heated at a rate of 300 K h^{-1} and air-quenched at 50°C intervals between 350 and 800°C to determine the possible reaction sequence. The resultant powders and heat-treated pellets were then analysed by X-ray diffraction (XRD) with a Philips diffractometer using CuK_α radiation from 2θ = 10 to 85° at a speed of 1° min^{-1}. The lattice parameter of the pure pyrochlore phase based on XRD was determined using a least-squares method and an internal gold standard over a high-angle region and at a low speed of 0·25° min^{-1}.

An extensive study of the $Bi_{3/2-x/2}Zn_{1+x}Sb_{3/2-x/2}O_{7-x}$ pyrochlore system was made by changing the zinc concentration from x = 0·1 to x = 1·2. As indicated by the formula, as the Zn concentration increases, Bi and Sb decrease to accommodate the Zn cations into the Bi and Sb sites to make a substitutional solid solution. These compounds were sintered at between 1035 and 1200°C for 4 h after calcining at 700°C for 4 h. Changes in the XRD pattern and the lattice constant were determined to indicate the range of Zn content in the pyrochlore structure and the lattice distortion associated with its incorporation.

Dense, polycrystalline ceramic pellets were fabricated from the calcined powders by uniaxial pressing at 250 MPa and firing for 4 h in air at 700–1200°C. The resulting microstructures in polished samples were examined using scanning electron microscopy (SEM, Camscan series 2) and transmission electron microscopy (TEM; Jeol 200CX operated at 200 kV). SEM samples were thermally etched at ~1050°C in air for around 10 min. Energy-dispersive spectroscopy (EDS) was performed using a LINK AN 10000 system with a Be-window detector. Pellet density was determined with a mercury densitometer.

3 Results and Discussion

3.1 Powder characterization

Chemical analysis of the natant solution (Table 1) after precipitation and filtering the wet solid showed that 99·2% of the starting materials was precipitated at a pH value of about 12. After drying the coprecipitated powder at 130°C, the white precipitate became yellowish probably due to the decomposition of $Bi(OH)_3$ at around 100°C.[10] Although the decomposition temperature of bismuth hydroxide is around 415°C,[14] it starts to lose water to form BiO(OH), and subsequently Bi_2O_3 when heated to 100°C.[10]

Figure 2(a) shows the TG–DTA curves of the mixed oxides of $3Bi_2O_3$–$3Sb_2O_3$*–4ZnO prepared via the solid-state reaction. The exothermic peak at approximately 550°C is thought to be due to oxidation of antimony oxide as the TG shows a weight gain around this temperature. Carnelley and Walker[15] showed that pure Sb_2O_3 undergoes a weight gain between 400 and 600°C due to oxidation. In addition, Kim *et al.*,[16] report that pure Sb_2O_3 shows a sharp exothermic peak due to oxidation of Sb_2O_3 at about 530°C and also that in ZnO doped with 2·0 mol% Sb_2O_3, this exothermic peak occurs at a lower temperature. In addition to this peak, two smaller exothermic peaks were observed at temperatures of between 500–600°C and 700–800°C. The cause of these two peaks was determined by XRD on samples heated to temperatures either side of each peak using identical conditions as for the thermal analyses. The former peak was due to the formation of $24Bi_2O_3$.ZnO ($Bi_{48}ZnO_{73}$, JCPDS card no. 26-230) and the latter was because of formation of pyrochlore. The DTA curve fell in an endothermic direction indicating that melting occurred above 850°C, probably due to unreacted Bi_2O_3 (m.p. 825°C).

Table 1. ICP-AES chemical analysis of solutions after precipitation at pH 12.

Element	*Amount ($\mu g\ ml^{-1}$)*	*Accuracy ($\mu g\ ml^{-1}$)*
Zn	9	±2
Bi	<1	–
Sb	57	±3

*Antimony III oxide oxidizes to antimony V oxide and enables formation of the $Bi_{3/2}ZnSb_{3/2}O_7$ pyrochlore formula.

Figure 2(b) shows the TG–DTA curves of the coprecipitated mixture. No weight loss was observed since any possible hydroxides present were removed upon drying at 130°C for 24 h. The exothermic peak at about 400°C was considered to be due to the formation of antimony IV oxide (Sb_2O_4). Another exotherm at 570°C is due to the crystallization of pyrochlore directly from the coprecipitated powders.

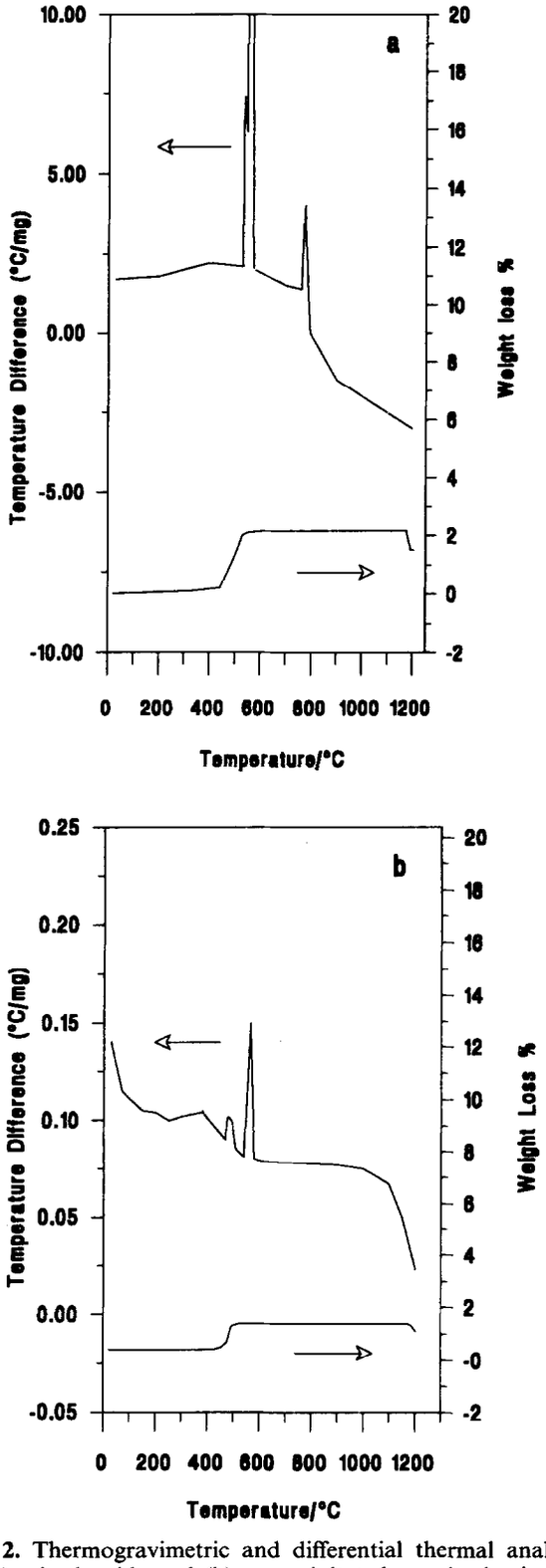

Fig. 2. Thermogravimetric and differential thermal analysis of (a) mixed oxide and (b) coprecipitated powder having an atomic ratio of Bi:Zn:Sb = 3:2:3. Note that DTA figures in (a) and (b) have different scales.

Subsequently, the DTA curve fell in an endothermic direction, after approximately 1000°C.

XRD analysis of the calcined mixed oxide powder [Fig. 3(a)] not only revealed pyrochlore but also β-Bi_2O_3, Sb_2O_4, ZnO and $Bi_{48}ZnO_{73}$ (BZ). However, XRD of the calcined coprecipitated powder [Fig. 3(b)] showed only single phase pyrochlore due to the higher reactivity of the coprecipitated powder. SEM images of these powders (Fig. 4) reveal that after calcination they consist of fine (sub micrometre) ultimate particles although in both cases the powders are highly agglomerated due to the calcination process. In addition, coprecipitated powders [Fig. 4(b)] have spherical and uniform particle shape.

3.2 Reaction sequence

XRD of crushed pellets of uncalcined powder [Fig. 5(a)] revealed no reaction of the mixed oxides up to ~550°C, with the appearance of $24Bi_2O_3.ZnO$ (BZ) being detected [reaction (3)] above 550°C. The formation of this compound produced the exothermic peak in the DTA [Fig. 2(a)]. At higher temperature, 700°C, the amount of BZ increased. This phase must arise because of poor mixing (heterogeneity) of the mixed oxide powders so that locally regions rich in Bi_2O_3 can react with ZnO to give BZ. Subsequently, at temperatures between 700 and 750°C, the BZS pyrochlore compound started to form from the reaction of BZ with the antimony oxide and unreacted ZnO and Bi_2O_3 [reaction (4)] or BZS compound may simply occur as in reaction (5) by reaction of the oxides after decomposition of BZ. Finally, nearly pure pyrochlore phase was observed at around 800°C, consistent with the DTA exotherm at 700–800°C [Fig. 2(a)].

$$24Bi_2O_3 + ZnO \xrightarrow{>550°C} Bi_{48}ZnO_{73} \quad (3)$$

$$Bi_{48}ZnO_{73} + 6Bi_2O_3 + 30Sb_2O_4 + 39ZnO + 15O_2 \xrightarrow{700–750°C} 40Bi_{3/2}ZnSb_{3/2}O_7 \quad (4)$$

$$3Bi_2O_3 + 3Sb_2O_4 + 4ZnO + 3/2O_2 \xrightarrow{500–550°C} 4Bi_{3/2}ZnSb_{3/2}O_7 \quad (5)$$

While intermediate reactions lead to pyrochlore formation in the mixed oxide powder, coprecipitated powder reacts directly to form pyrochlore at around 550°C without forming any intermediate compounds [reaction (5)] [Fig. 5(b)]. The formation of pyrochlore from coprecipitated powder gave an exothermic DTA peak at about 570°C [Fig. 2(b)]. The low formation temperature of pyrochlore in the coprecipitated powder can be attributed to the homogeneity of the coprecipitated powder [Fig. 4(b)]. Atomic-scale mixing of the components is considered to be attained in

coprecipitation. Consequently, the improved homogeneity and enhanced reactivity will decrease the diffusion path and encourage the reaction of BZS pyrochlore at lower temperatures.

3.3 Characterization of BZS pyrochlore

$Bi_{3/2}ZnSb_{3/2}O_7$ is isostructural with the pyrochlore type having general formula $A_2B_2O_7$. Its XRD peak data are listed in Table 2. Based on these results, $Bi_{3/2}ZnSb_{3/2}O_7$ was determined to have a cubic pyrochlore structure with the lattice parameter a_0 = 10·442 ± 0·001 Å. Inada[17] found a_0 for BZS pyrochlore to be 10·45 Å. Since XRD of BZS pyrochlore did not show any superlattice reflections, the cations are randomly distributed over the A and/or B sites in the $A_2B_2X_7$ pyrochlore structure.

Pellet densities after holding for 4 h at 700–1200°C are shown in Fig. 6. Densities of the coprecipitated

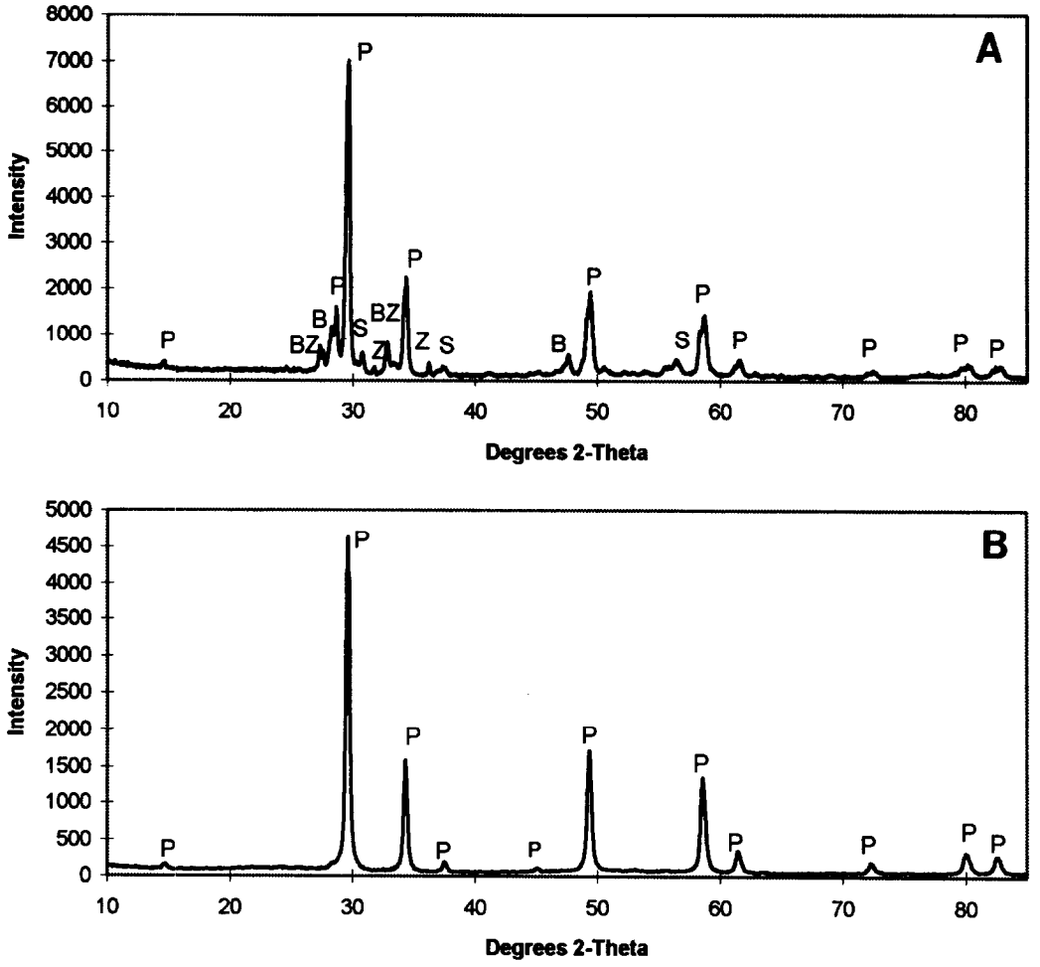

Fig. 3. XRD of calcined (a) mixed oxide and (b) coprecipitated powder. Calcination was for 4 h at 700°C. P = Pyrochlore, BZ = $Bi_{48}ZnO_{73}$, S = Sb_2O_4, B = β-Bi_2O_3 and Z = ZnO.

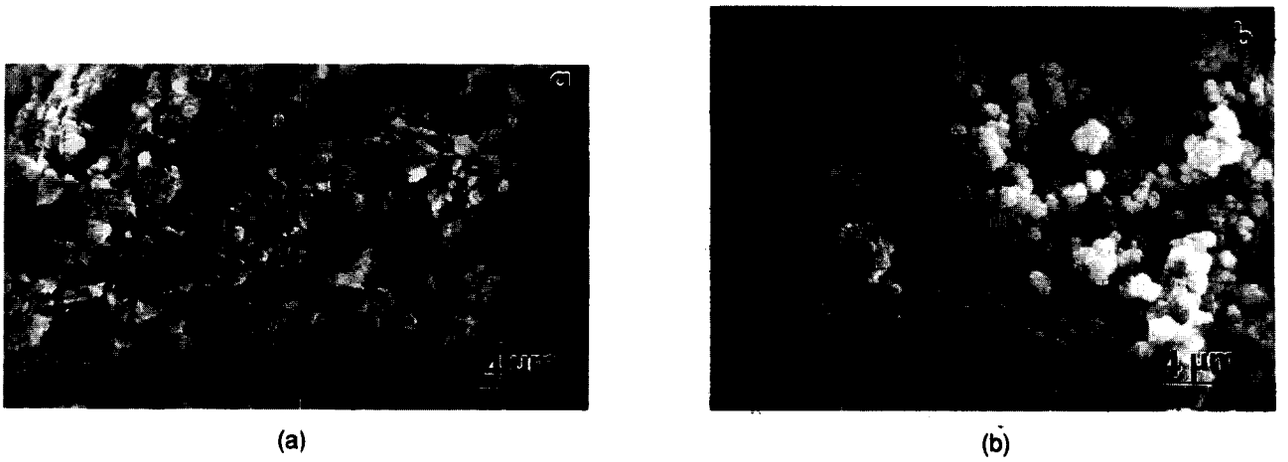

Fig. 4. SEM micrographs of (a) mixed oxide powder calcined at 700°C for 4 h and (b) coprecipitated powder calcined at 700°C for 4 h showing aggregated submicrometre primary particles.

powder pellets are generally higher since the starting powder has a lower ultimate particle size and more spherical particles, giving better packing. However, at the highest sintering temperature (1200°C) pellets from both powder types gave more than 90% of theoretical density, which is calculated as 7·86 g cm^{-3} from the X-ray results for a composition of $Bi_{3/2}ZnSb_{3/2}O_7$. At 1200°C the incomplete density of the pellets may be caused by the powder agglomerates (Fig. 4) and/or Bi_2O_3 and/or Sb_2O_3 volatilization since some weight loss was observed around this temperature in both powders (Fig. 2). Liquid-phase sintering is probable (Fig. 2), with melting occurring above 850°C for mixed oxide and 1000°C for coprecipitated powders. In addition, the sharp increase in density (Fig. 6) after approximately 1000°C suggests the occurrence of a liquid.

While SEM images of the dense pellets indicated only single pyrochlore phase [Figs 7(a) and 7(b)], TEM revealed occasional second phases at triple junctions consistent with liquid formation. Pellets made from coprecipitated powders have finer grains than those from mixed oxide. The second phases observed in the mixed oxide were generally crystalline and analysed as Bi_2O_3 by EDS [Fig. 8(a)], while in coprecipitated pellets these second phases were amorphous [Fig. 8(b)]. EDS analysis of the amorphous phase revealed Bi and a trace of K, a contaminant from the KOH used for precipitation which could flux the Bi_2O_3 and cause it to remain amorphous. No significant glassy phase was observed at the grain boundaries in both pellets, suggesting that any liquid is transient.[18]

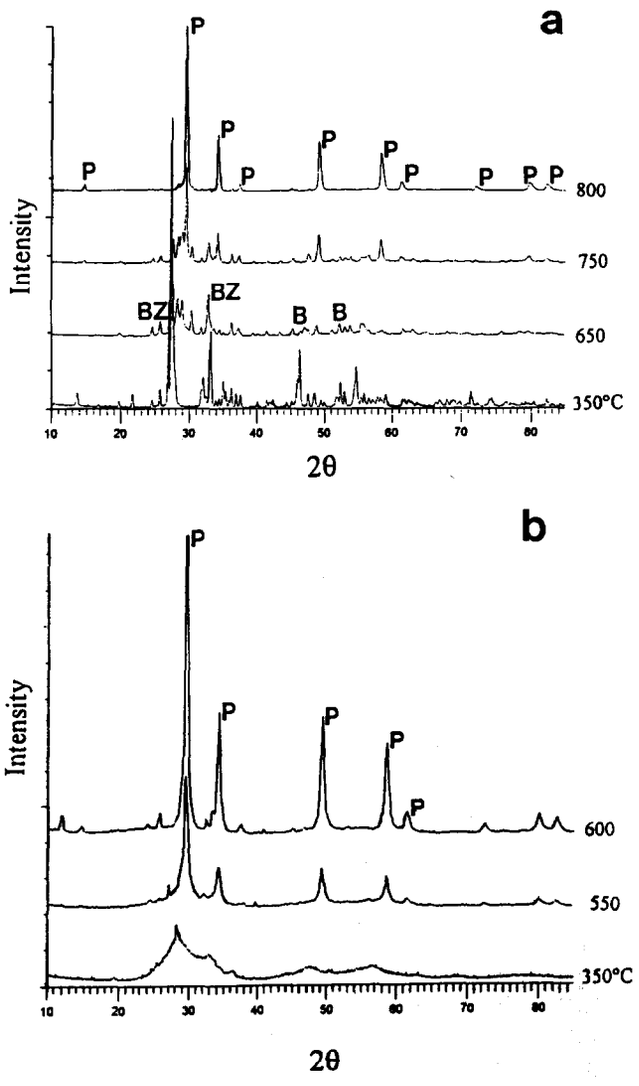

Fig. 5. XRD analysis of powders made from crushed pellets derived from (a) mixed oxide and (b) coprecipitation after air-quenching from different temperatures to determine the possible reaction sequence in both methods. P = Pyrochlore, BZ = $Bi_{48}ZnO_{73}$, B = Bi_2O_3.

Table 2. Powder XRD of $Bi_{3/2}ZnSb_{3/2}O_7$ pyrochlore

d (Å)	I/I_O	*hkl*
6·042	5	111
3·699	1	220
3·154	2	311
3·02	100	222
2·616	24	400
2·401	4	331
2·134	1	422
2·015	2	511
1·851	26	440
1·769	1	531
1·744	1	600
1·655	1	620
1·578	22	622
1·511	8	444
1·466	1	551
1·363	1	731
1·309	2	800
1·234	1	822
1·201	6	662
1·17	5	840

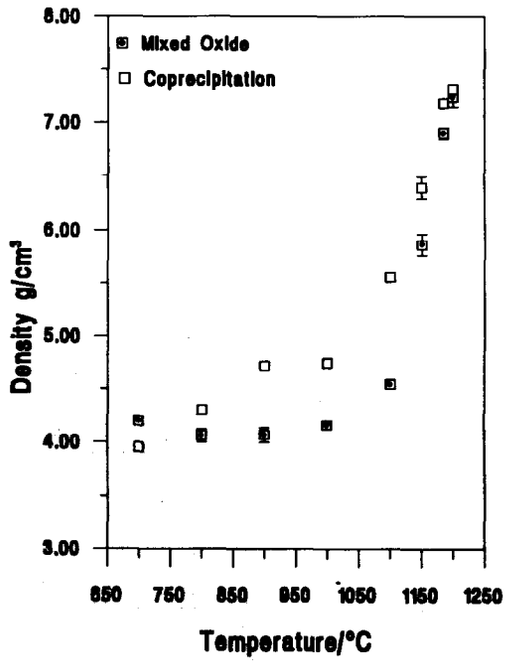

Fig. 6. Density of mixed oxide and coprecipitated pellets held for 4 h at temperature.

3.4 Zn cation incorporation into the BZS pyrochlore

XRD of Zn-doped samples is shown in Fig. 9 for $Bi_{3/2-x/2}Zn_{1+x}Sb_{3/2-x/2}O_{7-x}$ pyrochlore for x from 0·1 to 1·2. During incorporation of the Zn cation into the pyrochlore structure the spinel phase with the formula $Zn_7Sb_2O_{12}$ (beta spinel, JCPDS card no. 36-1445) forms and increases with greater Zn concentration. Figure 10 shows the relative peak intensities of the spinel (311) reflection, corresponding to a 3·577 Å d-spacing, and the BZS pyrochlore (400) reflection, which corresponds to a d-spacing of approximately 2·60 Å, as a function of excess Zn concentration, x. This gives a semi-quantitative measure of the spinel-to-pyrochlore ratio[19] and reveals that as the amount of Zn doping increases, the spinel percentage also increases. Consequently, it appears that increasing Zn concentration to replace Bi and Sb in the BZS pyrochlore was unsuccessful. Instead, spinel and Bi_2O_3 liquid formed along with pyrochlore of undefined composition.

The microstructure of the Zn-doped compound, after quenching from the sintering temperature, where $x = 1·2$ (Fig. 11), revealed not only pyrochlore and spinel phases, but also some Bi-rich phase present. This is consistent with reaction (1) where BZS pyrochlore in ZnO varistors takes the ZnO from the bulk matrix and transforms to spinel and liquid

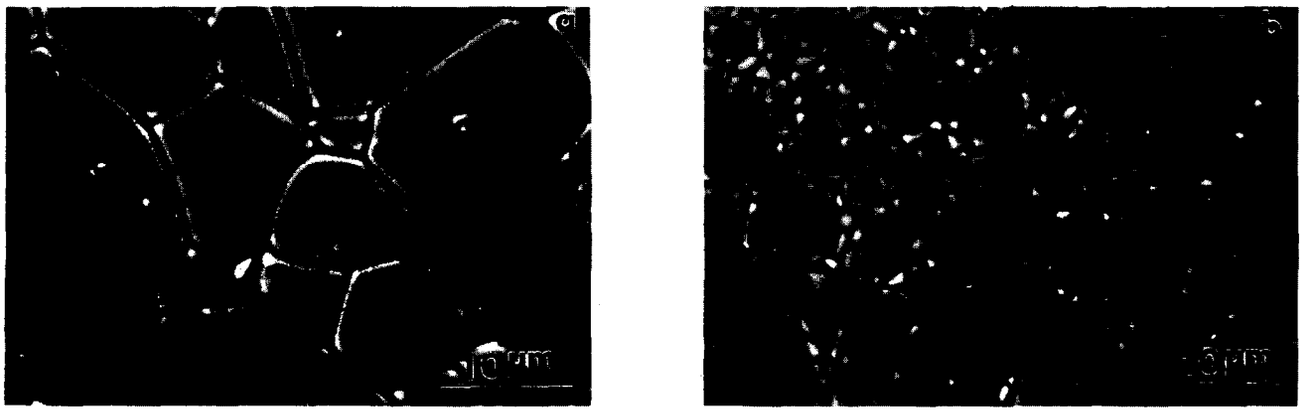

(a) (b)

Fig. 7. (a) Sintered mixed oxide pellet after 4 h at 1200°C showing only large (5–20 μm) single-phase grains. (b) Coprecipitated pellet after 4 h at 1200°C showing pyrochlore phase and finer (3–10 μm) grain structure.

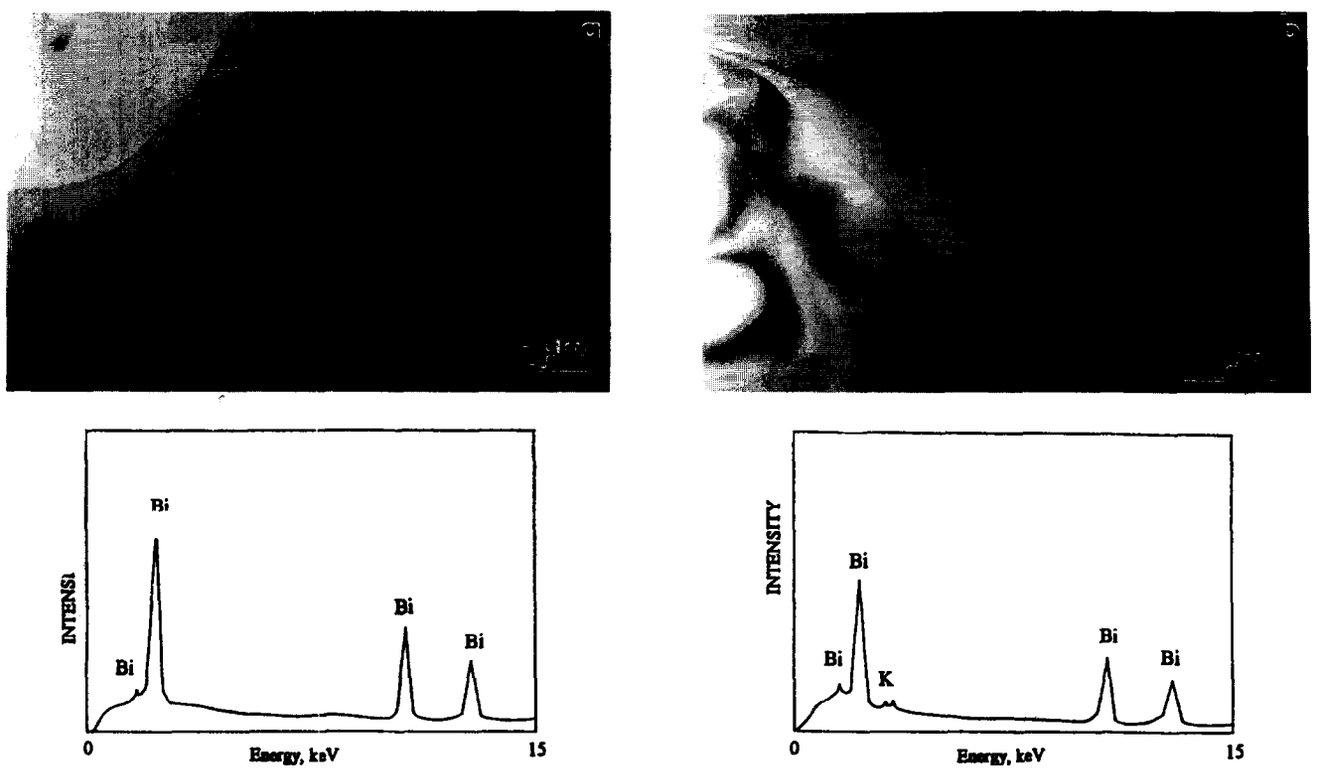

Fig. 8. (a) Bright-field (BF) TEM image of sintered mixed oxide pellet after 4 h at 1200°C showing crystalline second phase at grain junction. EDS analysis suggests the second phase is Bi_2O_3 (O is not detected). (b) TEM micrograph of coprecipitated pellet after 4 h at 1200°C showing glassy phase at triple junctions. EDS analysis reveals K as well as Bi.

Bi_2O_3.[8] Inada[8] showed that BZS pyrochlore reacts easily with ZnO to produce spinel and Bi_2O_3 liquid. SEM of this compound revealed large black (10–50 μm) spinel grains in the grey/white pyrochlore/Bi-rich phase matrix. Well developed faceted spinel grains indicative of crystallization from a liquid phase can be seen in the pyrochlore matrix [Fig. 11(a)]. In addition, spinel grains were frequently observed containing pyrochlore and Bi-rich phases [Fig. 11(b)].

TEM examination of Zn-doped samples sintered for 4 h at 1035°C reveals a range of grain sizes and additional intergranular phases (Figs 12 and 13). The TEM reveals the small pyrochlore grains (1–2 μm), large spinel grains (15–35 μm from SEM, Fig. 11) and impure Zn/Sb containing δ-Bi_2O_3 crystals (indicated by electron diffraction). Inada[8] found that Bi-rich liquid phase dissolves a large amount of Zn but much less Sb. δ-Bi_2O_3 is a high-temperature polymorph having a cubic structure and it completely surrounds the pyrochlore grains, suggesting that when liquid it was fully wetting.

In summary, addition of Zn to $Bi_{3/2}ZnSb_{3/2}O_7$ pyrochlore (and lower Bi and Sb) is observed to encourage it to transform to spinel with associated formation of Bi_2O_3-rich liquid which crystallizes to δ-Bi_2O_3 on cooling, rather than causing single-phase pyrochlore formation.

The lattice parameter of BZS pyrochlore increased with increasing Zn cation content (Fig. 14). Similar behaviour was reported by Inada,[17] who measured the lattice constant of BZS pyrochlore as a function of ZnO in the ZnO varistor system, and by Karanovic *et al.*,[20] who examined phase transformations in the system containing a mixture of varistor additives. The increased pyrochlore lattice parameter could be due to incorporation of Zn ions into the pyrochlore structure. The lattice parameter of BZS pyrochlore increased linearly up to $x = 0{\cdot}6$ but then a sharp increase was observed. The last three samples were sintered at lower temperatures (1035°C) than the initial ones (1200°C) since these compounds

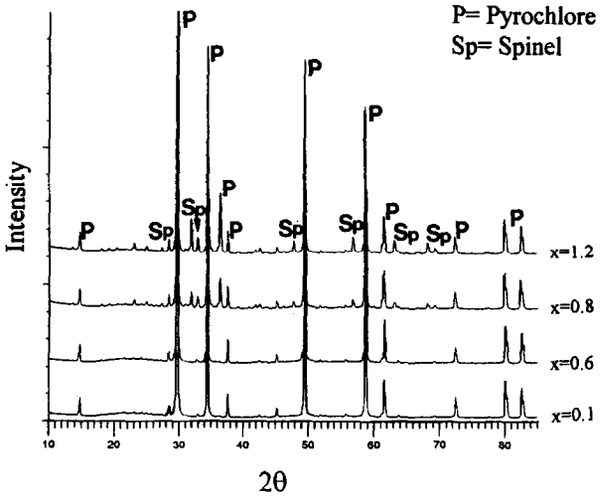

Fig. 9. XRD of $Bi_{3/2-x/2}Zn_{1+x}Sb_{3/2-x/2}O_{7-x}$ compositions sintered at 1200°C for $x = 0{\cdot}1$ and $0{\cdot}6$, and sintered at 1035°C for $x = 0{\cdot}8$ and $1{\cdot}2$. Sp = spinel, P = pyrochlore.

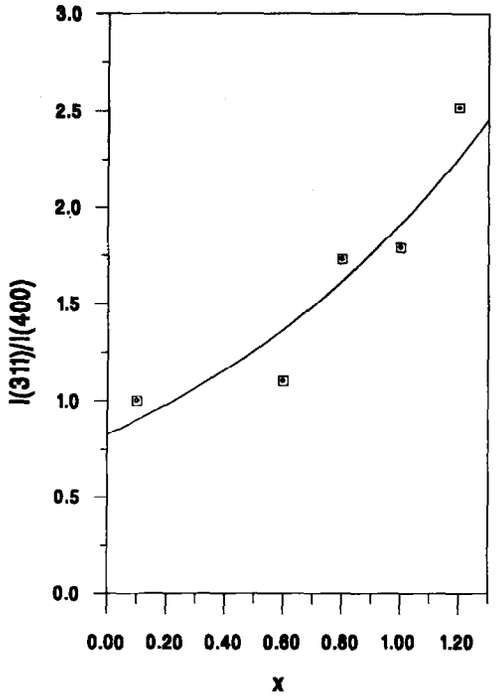

Fig. 10. Relative peak intensity ratio of spinel (311) to pyrochlore (400) as a function of excess Zn concentration, x, in $Bi_{3/2-x/2}Zn_{1+x}Sb_{3/2-x/2}O_{7-x}$.

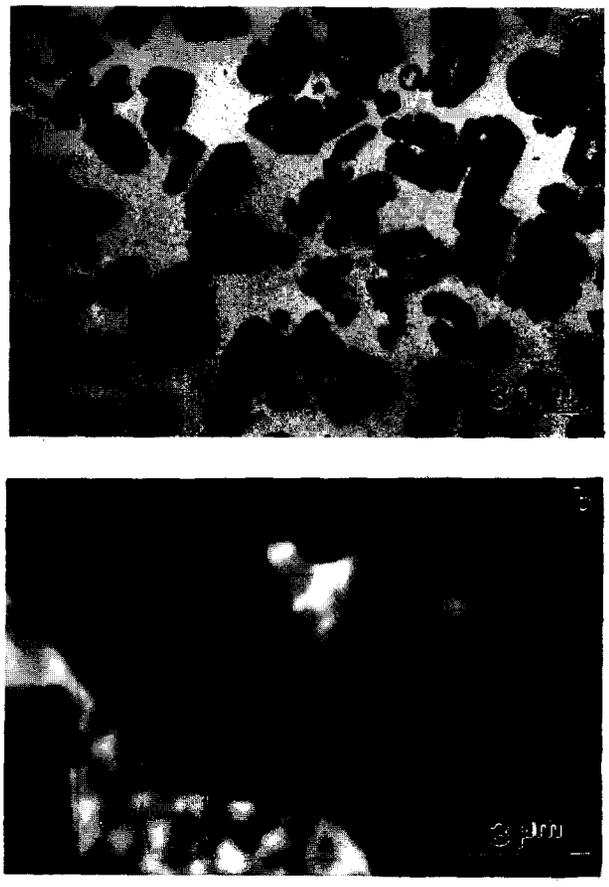

Fig. 11. Backscattered electron SEM images of a pellet of the $Bi_{3/2-x/2}Zn_{1+x}Sb_{3/2-x/2}O_{7-x}$ composition sintered at 1035°C for 4 h where $x = 1{\cdot}2$: (a) large faceted spinel grains, (b) grey and white pyrochlore and Bi-rich phases.

partially or mostly melt at the higher sintering temperature. This may have caused the sharp increase because at high temperatures more Bi_2O_3 evaporates and a higher proportion of the large Bi atom (radius 1·17 Å) at the lower sintering temperature would increase the lattice parameter.

4 Conclusions

(1) $Bi_{3/2}ZnSb_{3/2}O_7$ pyrochlore was prepared both by conventional solid-state reaction of mixed oxides and by a coprecipitation method.

(2) Investigation of the reaction sequence to pyrochlore via both methods showed that, in the mixed oxide method, pyrochlore is formed with the appearance of $24Bi_2O_3.ZnO$ compound above 550°C due to powder inhomogeneity. However, coprecipitated powder reacts directly to form pyrochlore at around 550°C due to atomic-scale mixing.

(3) Incorporation of Zn to replace Bi and Sb causes pyrochlore–spinel transformation rather than forming a single pyrochlore phase This is thought to be due to the reaction of pyrochlore with ZnO forming spinel and Bi_2O_3-rich liquid, as observed in ZnO varistors. In addition, Zn incorporation leads to an increased lattice parameter of BZS pyrochlore.

Acknowledgements

This work was sponsored by the Turkish Ministry of Education in the form of a scholarship (A.M.).

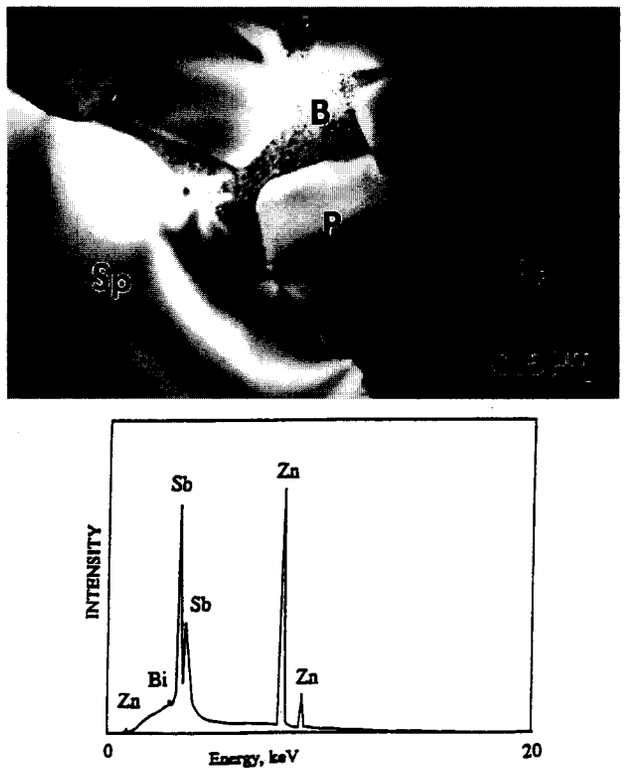

Fig. 13. BF TEM image of Zn-doped BZS pyrochlore ($Bi_{3/2-x/2}Zn_{1+x}Sb_{3/2-x/2}O_{7-x}$, x = 1·2) sintered for 4 h at 1035°C showing large spinel grains (Sp) with pyrochlore (P) and Bi-rich phase (B) with EDS analysis from spinel.

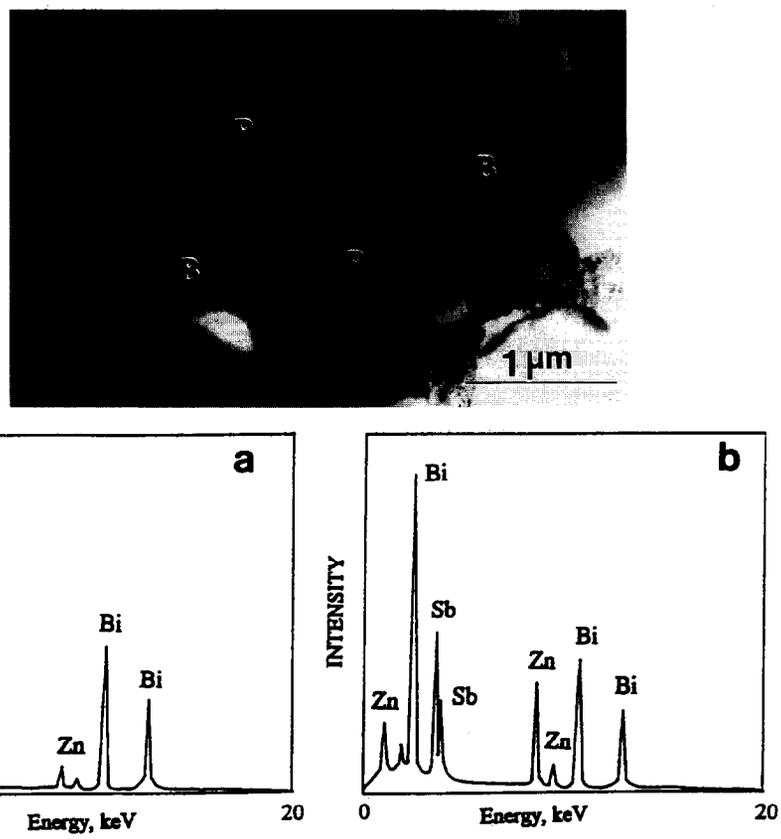

Fig. 12. BF TEM image of $Bi_{3/2-x/2}Zn_{1+x}Sb_{3/2-x/2}O_{7-x}$ composition where x = 1·2 sintered at 1035°C for 4 h with EDS analysis from (a) Bi-rich phase (B) and (b) pyrochlore (P).

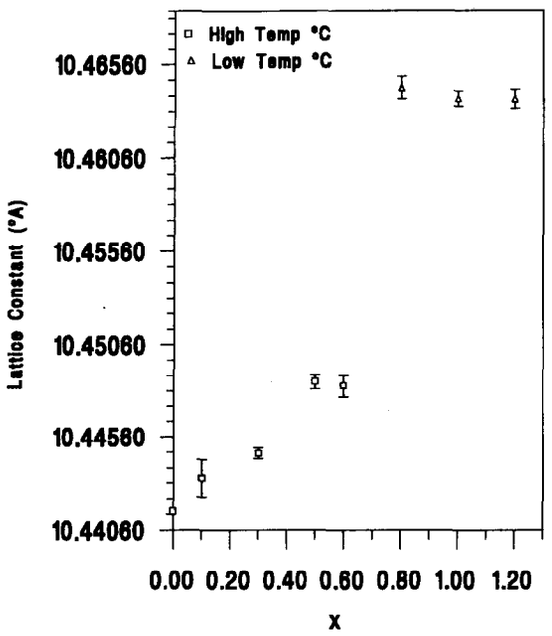

Fig. 14. Variation of the lattice constant with excess Zn concentration, x, in the $Bi_{3/2-x/2}Zn_{1+x}Sb_{3/2-x/2}O_{7-x}$ compositions sintered at 1200°C (first five samples) and at 1035°C (the last three samples) for 4 h.

References

1. von Gaertner, H., Die Kristallstrukten von Loparit und Pyrochlor. *Neues. Jahrb. Mineral Geol. Palaeontol.*, **61** (1930) 1–30.
2. Cook W. R. & Jaffe, H., Ferroelectricity in oxides of face-centered cubic structure. *Phys. Rev.*, **89** (1953) 1297–1298.
3. Sleight, A. W., New ternary oxides of mercury with the pyrochlore structure. *Inorg. Chem.*, **7**[9] (1968) 1704–1708.
4. Bystrom, A., X-ray analysis of $Ca_2Sb_2O_7$ and compounds of similar composition. *Ark. Kemi. Mineral Geol.*, **18A**[21] (1944) 1–8.
5. Kim, J, Kimura, T. & Yamaguchi, T., Sintering of zinc oxide doped with antimony oxide and bismuth oxide. *J. Am. Ceram. Soc.*, **72**[8] (1989) 1390–1395.
6. Subramanian, M. A., Aravamudan, G. & Subba Rao G. V., Oxide pyrochlores — a Review. *Prog. Sol. State Chem.*, **15** (1983) 55–143.
7. Karakas, Y. & Lee, W. E., Processing and phase evolution in a ZnO varistor prepared by oxide precipitation. *J. Brit. Ceram. Soc.*, **93**[2] (1994) 65–70.
8. Inada, M., Formation of nonohmic zinc oxide ceramics. *Jpn J. Appl. Phys.*, **19**[3] (1980) 409–419.
9. Olsson, E. & Dunlop, G. L., Characterization of individual interfacial barriers in a ZnO varistor material. *J. Appl. Phys.*, **66**[8] (1989) 3666–3675.
10. Durrant, P. J. & Durrant B., *Introduction to Advanced Inorganic Chemistry.* Longmans, Harlow, UK, 1962, pp. 771–772.
11. Durrant, P. J., *General & Inorganic Chemistry,* 3rd Edition. Longmans, Harlow, UK, 1952, pp. 548 and 684–685.
12. Vogel, A. I., *A Text Book of Macro & Semimicro Qualitative Inorganic Analysis,* 4th Edition. Longmans, Harlow, UK, 1955, p. 221
13. Hishita, S., Yao, & Shirasaki, S., Zinc oxide varistors made from powders prepared by amine processing. *J. Am. Ceram. Soc.*, **72**[2] (1989) 338–340.
14. Lide, D. R., *Handbook of Chemistry and Physics,* 73rd Edition. CRC Press, Boca Raton, FL, 1992–1993.
15. Carnelley, T. & Walker, J., The dehydration of metallic hydroxides by heat, with special reference to the polymerisation of the oxides, and to the Periodic Law. *J. Chem. Soc.*, **53** (1888) 59–101.
16. Kim, J., Kimura, T. & Yamaguchi, T., Sintering of Sb_2O_3-doped ZnO. *J. Mater. Sci.*, **24** (1989) 213–219.
17. Inada, M., Crystal phases of nonohmic zinc oxide ceramics. *Jpn J. Appl. Phys.*, **17**[1] (1978) 1–10.
18. Lee, W. E. & Rainforth, W. M., *Ceramic Microstructures, Property Control by Processing.* Chapman and Hall, London, 1994, pp. 46–47.
19. Wong, J., Microstructure and phase transformation in a highly non-ohmic metal oxide varistor ceramic. *J. Appl. Phys.*, **46**[4] (1975) 1653–1659.
20. Karanovic, L., Poleti, D. & Vasovic, D., On the possibility of pyrochlore phase formation in zinc oxide varistor ceramic. *Mater. Lett.*, **8** (1994) 191–196.